Photography Coupled with Self-Propagating Chemical Cascades: Differentiation and Quantitation of G- and V-Nerve Agent Mimics via Chromaticity

Xiaolong Sun,[†,∥,#] Alexander A. Boulgakov,[‡,#] Leilani N. Smith,[§] Pedro Metola,[§] Edward M. Marcotte,[*,‡] and Eric V. Anslyn[*,†]

[†]Department of Chemistry, [‡]Center for Systems and Synthetic Biology/Institute for Cellular and Molecular Biology, Department of Molecular Biosciences, and [§]Advanced Research Initiative, University of Texas at Austin, Austin, Texas 78712, United States

[∥]Bioinspired Engineering and Biomechanical Center, The Key Laboratory of Biomedical Information Engineering of Ministry of Education, School of Life Science and Technology, Xi'an Jiaotong University, Xi'an, 710049, P.R. China

S *Supporting Information*

ABSTRACT: Photography was employed for the quantitation and differentiation of G- and V-series nerve agent mimics with the use of self-propagating cascades. Fluoride anion and thiols, released from a G-nerve agent mimic (i.e., diisopropyl fluorophosphate) and a V-nerve agent mimic (i.e., demeton-S-methyl), respectively, were used to initiate self-propagating cascades that amplify fluorescence signals exponentially in a ratiometric manner. A homemade LEGO dark-box, a cell phone, and 96-well plates were employed to collect photographs of the fluorescence response to the analytes. The photographic images were digitally processed in the 1931 xyY color space using a watershed and morphological erosion algorithm to generate chromaticity vs concentration calibration curves. We show that the two different amplification routines are selective for their analyte class and thus successfully discriminated the G- and V-series nerve agent mimics. Further, accurate concentrations of the analytes are determined using the chromaticity and LEGO approach given herein, thus demonstrating a simple and on-site constructible/portable device for use in the field.
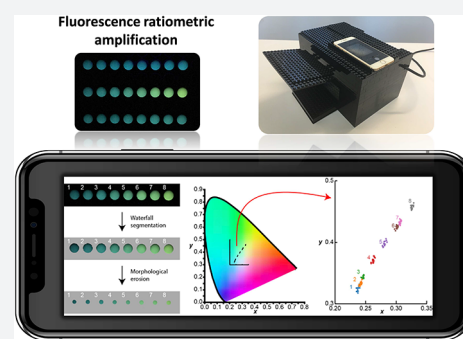
INTRODUCTION

Nerve agents are among the most lethal chemical agents developed for military use. They are divided into two types: G-series and V-series, of which the former are phosphoryl fluorides, such as sarin (GB), soman (GD), and tabun (GF), while the latter are phosphoryl thiols, such as O-ethyl-S-(2-diisopropylaminoethyl)methylphos-phonothioate (VX), O-iso-butyl-S-2-diethyl-aminoethyl methyl-phosphonothioate (RVX), and O-butyl-S-2-diethyl-aminoethyl methylphospho-nothioate (CVX) (Figure 1). The species are odorless and tasteless, and possess very low median lethal doses (LD_{50} from 0.069 mg/kg to 117.9 mg/kg for G-nerve agents, and 0.0082 mg/kg to 1.402 mg/kg for V-nerve agents).[1,2] Due to the increased toxicity and lower volatility compared to the G-agents, the LD_{50} of V-agents is 10 times lower, and thus these agents are more dangerous than G-nerve agents. Both V- and G-agents are threats for humanity, particularly in a modern world facing the very real possibility of terrorist attacks. This threat has been a motivation for research into the development of user-friendly and sensitive chemosensors for such agents.[3] However, to date, few strategies have been reported for the detection of nerve agents demonstrating high sensitivity and quantitative accuracy, and with the ability to discriminate between the V- and G-agents, as well as an ease of operation that makes the entire analysis field deployable.
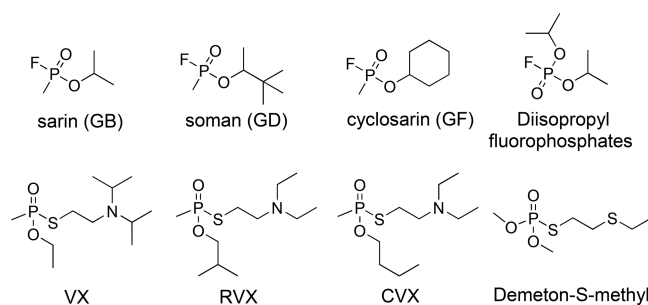
Figure 1. Structures of chemical warfare nerve agents and mimics. The common fluoride-containing G-series nerve agents and the mimic: diisopropyl fluorophosphates (DFP); the common sulfur-containing V-series nerve agents and the mimic: demeton-S-methyl (DSM).

In terms of optical sensing methods currently being explored, exponential signal amplification offers significant advantages to conventional detection, such as significantly larger diagnostic signals, increased sensitivity, and accompanying lower limits of detection (LOD), which continually inspire the development of new approaches in this field.[4] In the past

decade, a series of self-propagating cascades for analyte quantitation and signal amplification in response to H_2O_2, fluoride, and thiols were developed.[5−9] One equivalent of analyte triggers the cascades to generate hundreds to thousands of equivalents of further triggers, and thus the signals generated grow exponentially. In previous studies, we designed and developed self-propagating cascades to detect fluoride and thiols, as well as their application in sensing of G- and V-type phosphoryl nerve agent mimics by monitoring the fluoride/thiol products (Figure 2).[10−12]
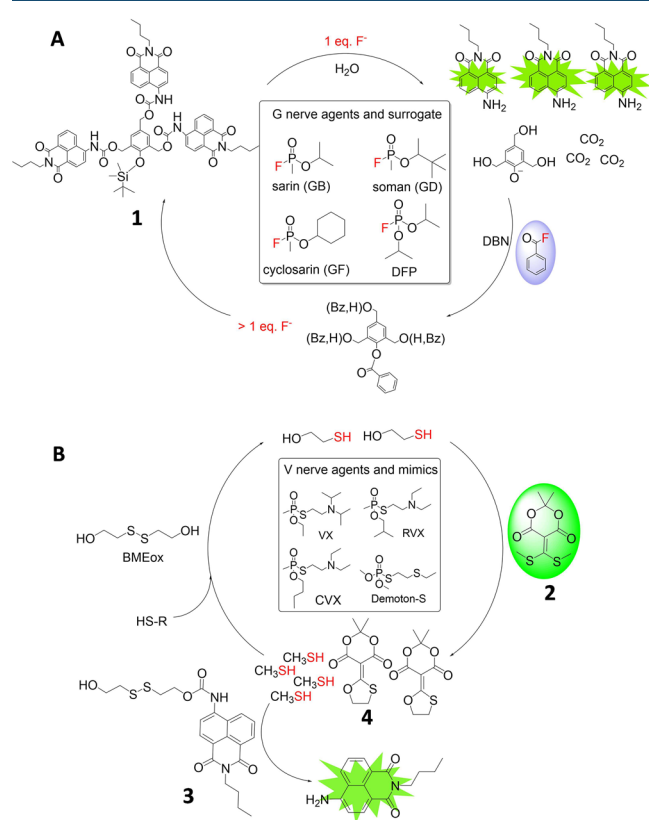
Figure 2. Self-propagating cascades for optical sensing of G- and V-nerve agent mimics. (A) Self-propagating cascade employing benzoyl fluoride (BF) as a latent source of fluoride for signal amplification and optical detection of fluoride and phosphoryl fluoride nerve agent mimic DFP.[10] (B) Self-propagating protocol employs a Meldrum's-acid-based conjugate acceptor (2) as a latent source of thiol for signal amplification, as well as optical detection of thiols and thiophosphate nerve agent mimic DSM.[12]

These approaches, as well as many others, exploited ratiometric signaling. Ratiometric fluorescence sensing has the potential to provide high sensitivity and inherent reliability due to the self-calibration provided by monitoring two (or more) emissions.[13] In the exploration of ratiometric fluorescence probes, scientists such as Nagano[14−16] and Qian[17−19] have made contributions to the sensing of transition metals. Among many of their ratiometric designs, the 4-aminonaphthalimide chromophore is widely employed due to its advantageous photophysical and photochemical properties, synthetic accessibility, and tunable internal charge transfer (ICT).[20] Hence, in the two self-propagating cascades introduced above, we employed 4-aminonaphthalimide via functionalizing the electron donating 4-amine moiety. The result is fluorometric red shifts within the visible color region

after reaction of the probe and the proper analyte due to a recovery of a "push−pull" π-electron system, which was visibly seen as a different color of emission and could be captured via photography for color analysis (vide infra).

Traditionally, to record and interpret the optical changes, spectroscopy measurements such as fluorescence spectroscopy, ultraviolet−visible absorption spectroscopy, X-ray photoelectron spectroscopy, circularly dichroism spectropolarimetry, etc., utilizing sophisticated instruments are required. Consequently, the instrumentation is usually costly, not readily field deployable, and its operation can be time-consuming. Thus, simple, efficient, and ideally integrated systems are in great demand.[21]

To answer this need, we herein report an image analysis pipeline to perform ratiometric fluorescence sensing using a common cellular phone[22−24] and a housing built from LEGO.[25] Briefly, photographic images of the reactions in wells of a 96-well plate are digitally processed to identify the individual reaction wells, and their pixel values are sampled. Pixel chromaticities for each well are quantitatively mapped onto the CIE 1931 xyY color space.[26] Chromaticities from calibration wells with known analyte concentrations form a calibration curve in the color space against which the other reactions' chromaticities are then compared. This is sufficient to infer analyte concentration in each reaction. We thus combine ubiquitous digital photographic technology, a simply constructed box, with our fluoride and thiol self-propagating protocols to create portable devices for use in the discrimination and quantitation of G- and V-nerve agent mimics.

■ RESULTS AND DISCUSSION

Procedure and Tools for Photo Images. As an initial test of the fluoride self-propagating cascade, we used TBAF as the trigger and observed the fluorescence produced by the cascade. We then tested the cascade for the detection of DFP, using the fluoride released from the chemical reaction between DFP and a previously reported oximate on a resin in *tert*-butyl methyl ether (TBME).[10] For an initial test of the thiol self-propagating cascade, we used butanethiol as the trigger. For the detection of DSM, we used the thiol released from its hydrolysis in pH 12.0 buffer at 60 °C.[12] In all cases, the cascades performed as previously reported.

As a means to generate quantitative protocols, the self-propagating cascades were run to a set amount of time after triggering with their analytes. The reactions were then transferred to 96-well plates, and the plates were exposed to UV light and photographed by an iPhone (vide infra). Further, to prove the utility of self-propagating cascades in signal enhancements, control experiments just containing the fluorescence probes were carried out side-by-side with the cascades. In addition, to prove the orthogonality of our methodology, interference of the other nerve agent was tested in each cascade (vide infra).

In our previous studies, a 96-well plate spectrofluorimeter was set at a specific excitation wavelength, and emission was recorded at a specific wavelength. The sensitivity and accuracy from a commercially available instrument are, of course, excellent. However, such a device is not field deployable. Thus, we took a completely new approach, one that would replace a conventional 96-well plate reader, be inexpensive, and could be constructed in the field. To accomplish this, we turned to the use of a 96-well plate reader made from LEGO, thereby

making a dark-box (instructions for construction are given in the Supporting Information) to image and photograph the color of fluorescence from each well of the plate (Figure 3).
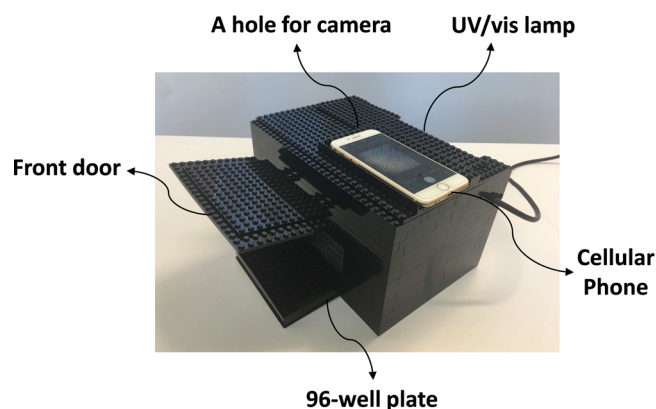
Figure 3. A homemade LEGO dark-box for imaging using a cell phone. The LEGO box is equipped with a UV/vis lamp, a hole for the iPhone camera, and guides for camera and plate placement.

Admittedly, we could have used a 3D-printer to generate the box. However, LEGO is a far easier medium from which to construct such a device. First, one does not need to generate a CAD file each time a new design is needed, and LEGO can be reconfigured rapidly and on-the-go to suit the design needs of the user. Lastly, LEGO can be disassembled into pieces easily housed in a portable bag.

Thus, the dark-box was equipped with a UV/vis lamp in the back, and a front door for placement of the 96-well plate onto an internal guide/ramp. In addition, there are LEGO edges on the top to guide the phone's placement, and a hole properly placed for the cellular phone's camera. The box is readily modified to accommodate any phone.

The nerve agent mimics were treated outside of the LEGO box to release fluoride/thiols completely, and then used as triggers for the self-propagating cascades. After signal amplification, we added them into a 96-well plate and then moved to the LEGO box. The well plate containing the samples was illuminated with an attached broad-band UV lamp, and photographs generated with an iPhone camera. The images were then exported for computational analysis (vide infra).

Sample Chromaticity Analysis from Photo Images. Each well of a 96-well plate was analyzed to obtain the reaction's chromaticity as follows. The top of Figure 4A is a representative image. First, we used the waterfall algorithm[27] to segment all fluorescent wells in the image. The waterfall algorithm is a hierarchical extension of the watershed algorithm that reduces oversegmentation. Briefly, the image is color-inverted and converted into grayscale, such that each fluorescent well is a dark object against a white background. It is useful to think of pixel values as elevation and the image as a topographic map with the wells acting as basins surrounded by a relatively flat landscape. Intuitively, the watershed algorithm identifies locations of the image as belonging to the same basin whenever drops of water placed at those locations flow toward the same minima. The waterfall algorithm improves on this by eliminating spurious adjacent basins that are merely parts of a larger one. After waterfall segmentation, we perform a final filter on basins by discarding pixels whose values deviate from background noise less than
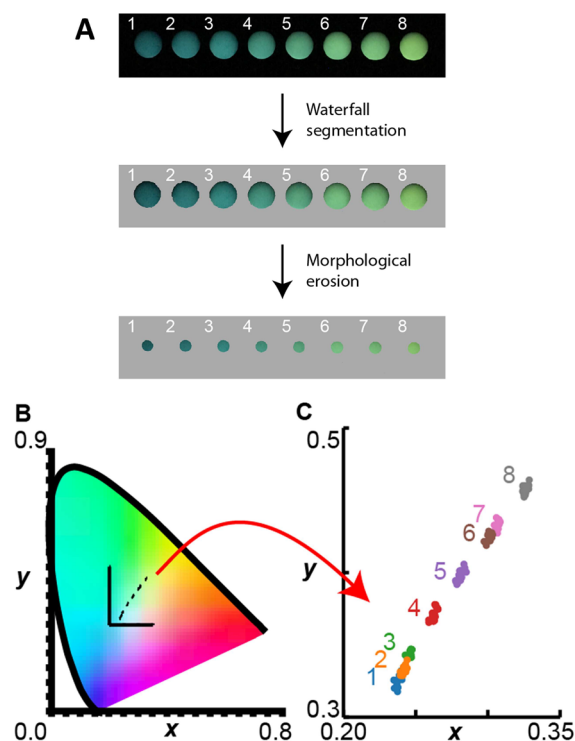
Figure 4. Fluorescent cascade reaction chromaticity quantitatively corresponds to analyte concentration (DSM, numbers 1 to 8:0.0, 0.5, 1.0, 1.5, 2.0, 2.5, 3.0, 3.5 ppm respectively). Fluorescent wells (A, top) are identified using the waterfall algorithm (A, middle) and morphologically eroded to avoid edge effects to capture the most representative well colors (A, bottom). (B) The CIE xyY color space decomposes colors into two chromaticity components represented by the x and y axis, and one luminosity component Y (not shown). Pixels from eroded wells are mapped into the color space (inset). Color space graphic adapted from Wikipedia. (C) The inset figure in (B) zoomed out. Each well's pixels from (A) are clustered in $x-y$ coordinates around its representative chromaticity, defined as the median of all well's pixels.

two standard deviations. The final result is that only the large fluorescent wells remain (Figure 4A, middle). To obtain the most representative pixels in each for its reaction, morphological erosion[26] (Figure 4A, bottom) was applied to each well to exclude pixels near the periphery of each well: any pixel within a certain distance of the well boundary was removed from consideration. The color values for the representative pixels in each well were decomposed per the CIE 1931 xyY color space (Figure 4B)[26] into the two chromaticity components x and y and the luminosity component Y. Figure 4C plots chromaticities for pixels randomly subsampled from each of the (eroded) calibration wells. We take the median of all pixels from each well to be that well's *representative chromaticity*. We thus abstracted each reaction into a two-dimensional coordinate in xy chromaticity space.

Such that anyone can reproduce this work, as well as apply our methods to other reactions in 96-well plates, we have uploaded our code, a sample image, and a full demonstration of our analysis to our GitHub at https://github.com/marcottelab/Titiwai.[28] The demo notebook included can be easily adapted to analyze new images. The details are discussed in the Supporting Information.

To test whether the position in the plate, and therefore also the position within the dark box, affected the chromaticity, we

carried out an experiment using four fluorescence dyes with different emissions, but placing them in random positions (Figure S1). It was found that the chromaticities of each fluorophore were independent of the position within the plate.

There are some self-correcting features of our LEGO box, UV lamp, and iPhone device. First, because we are not using the Y portion of the xyY color space, the luminosity (i.e., brightness) of the images does not matter. Thus, the gain on the phone and the flux from the lamp are not relevant. It is only important that the same lamp and phone is used to generate the calibration curves and to analyze the sample. Each different lamp would put out slightly different broad band irradiation for excitation, and thus one expects different colors of emission. Further, each phone has a different CCD, and while brightness is now controllable with an iPhone, each phone is still expected to give slightly different chromaticity. Second, because the phone does not capture UV light, the lamp can be kept on during the analysis, and only the color of emission is recorded. This is different than a standard plate reader that excites the sample, has a delay, and then reads emission.

A crucial and very useful property of the CIE 1931 xyY color space is that a mixture of any two light sources with differing chromaticities—i.e., any two points within the spectra locus of Figure 4B—will itself necessarily lie on the line between the two points.[26] Representative chromaticities from our calibration wells tended to be linearly distributed across all experiments, as visually evident in Figure 4C. In this example, the calibration wells contain increasing concentrations of DSM, which map to a linear curve in xy chromaticity space. We hypothesize that this linearity is a natural consequence of ratiometric fluorescence: each of the two-fluorescent species present in each reaction emits a particular chromaticity, and the combined fluorescence is a mixture of these chromaticities.

Once representative chromaticities have been measured for the calibration wells, they are used to construct a calibration curve in chromaticity xy space. This curve is a piecewise linear interpolation between each successive calibration chromaticity (Figure 5). We use piecewise linear interpolation instead of a single linear interpolation across all points because the CIE 1931 xyY color space is not uniform:[26] identical color differences in disparate regions of the color space do not correspond to identical Euclidean distances. Color spaces attempting uniformity have been developed; however, none of them can entirely avoid this problem.[26] Therefore, a piecewise interpolation hedges against this error.

Once a calibration curve was constructed, it was used to infer each reaction's analyte concentration from its representative chromaticity (Figure 5). First, the nearest line segment of the calibration curve to the representative chromaticity of interest is found. The representative chromaticity is projected to the calibration segment, and the ratio of distances to the two nearest calibration wells is used to interpolate between them. For example, an unknown analyte lying between two calibration wells of 1.0 and 2.0 ppm, and being 30% of the distance from the 1.0 ppm well is 70% × 1.0 + 30% × 2.0 = 1.3 ppm.

Photo Analysis for TBAF and DFP. Using the fluoride self-propagating cascade introduced above, we sought to use our chromaticity and photographic technique to quantitate TBAF and DFP concentrations. The emission signal generated in response to the addition of fluoride showed both an exponential decrease at 440 nm and an increase at 500 nm.[10]
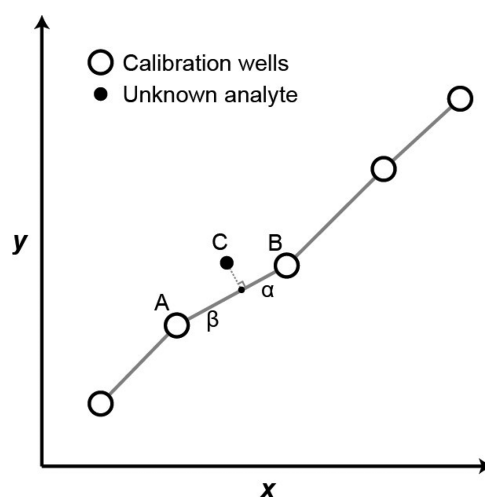
Figure 5. Schematic illustration for detection of unknown analytes. Calibration wells are used to construct a piecewise-linear calibration curve in xy color space (gray line segments). Chromaticity of unknown analyte C is projected onto the nearest line segment, in this case between calibration wells A and B. We linearly interpolate the concentration of C using the Euclidean distances α and β from the projected point to wells B and A, respectively, so that $[C] = \frac{\alpha}{\alpha+\beta}[A] + \frac{\beta}{\alpha+\beta}[B]$.

As can be seen from Figure 6A (inset), colors in row 2 shift with increasing doses of TBAF triggers. The fluorometric changes were recorded after a 10 min self-propagation in TBME, and then diluted with an equal amount of acetonitrile for fluorescence photo collection and color differences (blue to yellow), which are easily detected by the naked eye. We quantitatively analyzed these changes using the approach described above to infer analyte concentrations (Figure 6A). The representative chromaticities followed a linear trend in xy space with increasing TBAF concentrations.

In an additional experiment, a linear relationship was formed between TBAF (0–1.31 ppm) concentration and luminosity, with $R^2 = 0.98$ and LOD = 0.17 ppm ($3\sigma/\kappa$) (Figure S2B).[29] However, it was observed in the luminosity that the intensity of images triggered by targets more than 1.31 ppm reached a flat saturation due to a longer time's signal amplification (15 min) and the phone's ability to decipher brightness, but in color space the chromaticity continues to vary in a linear manner (Figure S2C). Thus, the concentration of samples within this range, can still be mapped by the chromaticity segment-method through piecewise linear interpolation. This is strong evidence that chromaticity is more informative than luminosity in measuring ratiometric fluorescence changes.

The control experiments that do not contain the self-propagating cascades (row 1 Figure 6A) show minor fluorometric changes occurring in response to TBAF, which highlights the importance of the self-propagating system for signal amplification. Equally important, these self-propagating cascades displayed nearly no color alteration in response to the addition of butanethiol (row 3 Figure 6A), which confirms the selectivity of our protocol for fluoride over thiol derivatives (i.e., other nucleophilic agents).

To further test the application of this photographic technology, we monitored the fluorescence changes of the images resulting from the self-propagating cascades in the detection of G-type nerve agent mimic DFP, along with any possible interference of VX nerve agent mimic DSM. We
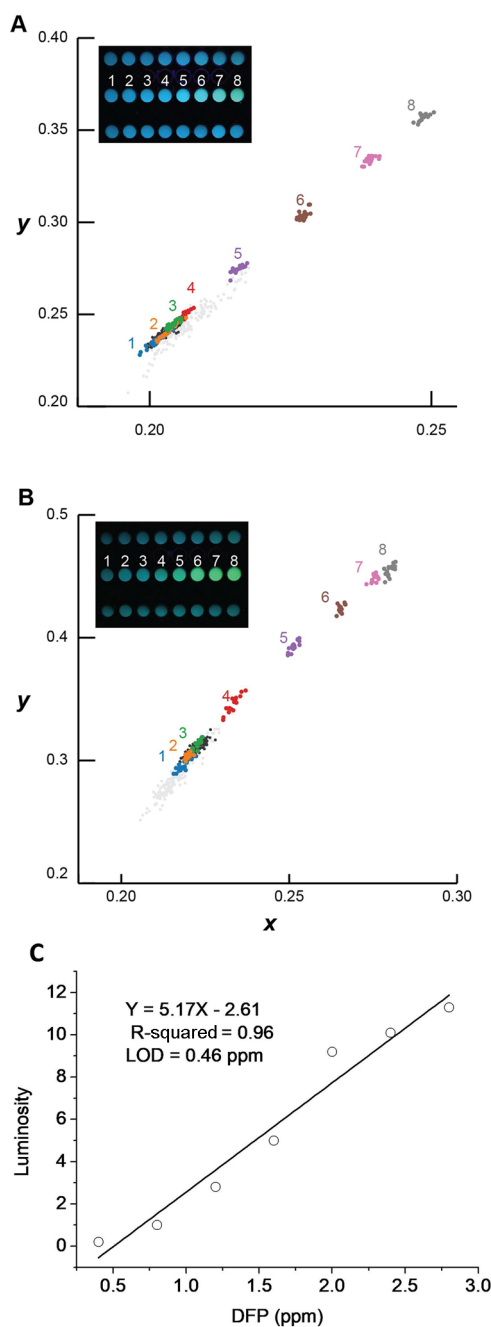
Figure 6. Fluorescence photo images; chromaticity for TBAF and DFP triggered self-propagating cascades. Row 1 is a control for analyte with only probe **1** present. Row 2 is for analyte under self-propagating cascades conditions. Row 3 is a control for interference via self-propagating cascades. (A, inset) TBAF titrations (0, 0.26, 0.52, 0.78, 1.05, 1.31, 1.57, 1.83 ppm) in row 1 and 2. Butanethiol (0−0.72 ppm) in row 3; (B, inset) DFP titrations (0, 0.4, 0.8, 1.2, 1.6, 2.0, 2.4, 2.8 ppm) in row 1 and 2. DSM (0−3.5 ppm) titrations in row 3; (A, B, graph) Chromaticities of randomly sampled well pixels. Pixels from row 1 wells are light-gray; pixels from row 3 wells are dark-gray. Row 2 wells are color-coded and numbered. (C) Linear relationship between fluorescence luminosities and DFP doses. Self-propagating cascades containing probe **1** (5 μM), DBN (20 μM), and BF (500 μM) were processed at a 10 min time point for TBAF and at a 20 min time point for DFP.

employed a previously reported resin-bound oximate to generate fluoride from aliquots of DFP,[10] followed by

quantitation using the **1**/BF self-propagating cascades. To start, solutions containing different amounts of DFP were mixed with the Wang resin-oximates in the presence of P$_4$-t-Bu base in TBME for 30 min, and after filtration, the filtrates were added to the self-propagating system for a defined time and then diluted with acetonitrile, followed by photography. Chromaticity data show that only DFP-induced fluoride anions led to distinct fluorometric transformation in a dose-dependent manner (Figure 6B, row 2). By contrast, slight to no signal change occurred in the control samples without fluoride self-propagating cascades (Figure 6B, row 1). Additionally, the fluoride self-propagating cascade for G-type agents did not respond to DSM which released thiols, showing its selectivity (Figure 6B, row 3). Likewise, luminosity data (Figure 6C) generated a linear curve for the relationship between DFP doses (0−2.8 ppm) and intensities in row 2 with $R^2 = 0.96$ and LOD = 0.46 ppm ($3\sigma/\kappa$), distinguishing the different amounts of fluoride produced from DFP when triggering the exponential fluorescence signal.

Photo Analysis for Thiol and DSM. Next, we triggered the system containing **2** and BMEox using butanethiol for a certain time, and then added fluorescence probe **3** for thiol sensing. As seen in Figure 7A, samples of self-propagating cascades in row 2 went through 20 min of self-amplification in the presence of various amounts of butanethiol (number 1−8, 0−3.15 ppm) in pH 10.0 buffer and then were diluted with pH 7.30 PBS buffer (50% DMSO) containing probe **3**. Noticeably, there were visible color switches from blue to yellow originating from the naphthalimide chromophore, reflecting different accumulations of thiols after self-propagating.

We then analyzed the photos by chromaticity and luminosity (Figure 7A and Figure S3). In the analysis of chromaticity, only wells 1−8 in Figure 7A row 2 displayed color changes in a linear progressive trendline, while control samples hardly exhibit chromaticity changes due to insufficient thiol (Figure 7A, row 1) or nonreactivity toward fluoride anion (Figure 7A, row 3). In terms of luminosity, a linear relationship exists between butanethiol concentration and intensity, with $R^2 = 0.98$ and LOD = 0.38 ppm ($3\sigma/\kappa$) (Figure S3), except that the luminosity signal in the presence of butanethiol (2.25 ppm) deviated from a linear curve, while the chromaticity of this concentration stayed within the linear trendline. This again highlights that luminosity is less reliable than chromaticity and hence can only be adopted as a supplementary diagnosis.

To evaluate the protocol in the detection of VX nerve agent mimic DSM, an experiment similar to the one for DFP was carried out using our thiol amplification routine (Figure 7B). First, aliquots of DSM (0−3.5 ppm) were stirred in an aqueous pH 12.0 solution at elevated temperature (60 ^{o}C) to release 2-(ethylsulfanyl)ethane-1-thiol and then incubated with the self-propagating cascade (at pH 10.0 buffer) for 20 min. Probe **3** was then added to the samples above for fluorescence sensing and imaging. Clear color differences can be observed in the samples containing moieties **2**, **3**, and BMEox (Figure 7B, row 2), while the controls showed minor changes toward DSM and DFP (Figure 7B, rows 1 and 3). Further, fluoride did not initiate the self-propagating cascade, demonstrating that the thiol cascade is selective for V-nerve agents over G-agents. Furthermore, chromaticity of the samples in row 2 showed a quantitative trend in the analysis of DSM, which can be potentially applicable as calibration for identification of unknown samples (Figure 7B, graph). As seen in Figure 7C, a linear relationship was also formed between DSM
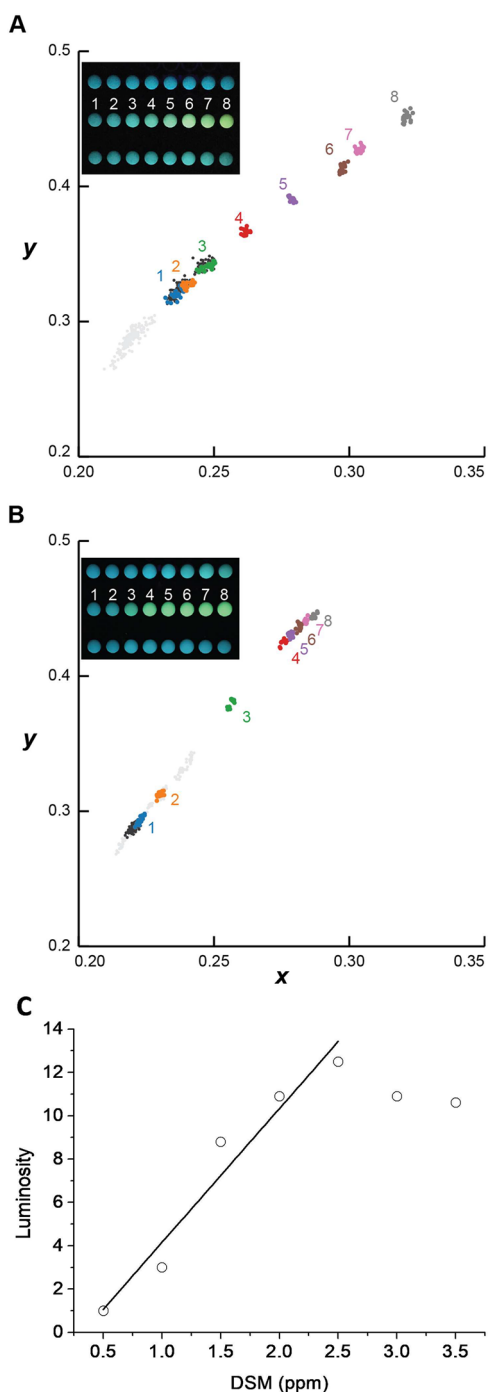
Figure 7. Fluorescence photo images; chromaticity for butanethiol and DSM triggered self-propagating cascades. Row 1 is a control for analyte titrations with only probe **3** present. Row 2 is analyte titrations under self-propagating cascades conditions. Row 3 is a control testing for interference via self-propagating cascades; (A, inset) Butanethiol (0, 0.45, 0.9, 1.35, 1.8, 2.25, 2.7, 3.15 ppm) in row 1 and 2. TBAF (0−9.1 ppm) in row 3; (B, inset) DSM (0, 0.5, 1.0, 1.5, 2.0, 2.5, 3.0, 3.5 ppm) in row 1 and 2. DFP (0−2.8 ppm) titrations in row 3; (A, B, graph) Chromaticities of randomly sampled well pixels. Pixels from row 1 wells are light-gray; pixels from row 3 wells are dark-gray. Row 2 wells are color-coded and numbered. (C) Relationship between fluorescence luminosities and DSM doses. Thiol self-propagating cascades contain **2** (0.16 mM), BMEox (0.16 mM) in pH 10.00 (20% acetonitrile cosolvent) at a 20 min time point.

concentration and luminosity in the range of 0−2.5 ppm, but higher concentrations of DSM deviated from this trend.

We have thus demonstrated that photographic diagnostic methods coupled with self-propagating cascades can be applied successfully for detection of a fluoride and fluorophosphate nerve agent mimic, as well as a thiol and thiophosphate nerve agent mimic, respectively. We displayed the sensitivity and selectivity of each cascade for its corresponding analyte through photography. In both cases, chromaticity proved more accurate and informative than luminosity (with luminosity potentially as a supplemental source of information). On the basis of these results, our methodology for analyzing self-propagating cascades through fluorescence chromaticity can be used to differentiate and quantitate G- and V-nerve agent mimics.

Photographic Detection of Unknown Samples. Rapid and precise detection and identification of unknown samples in the field by a portable device is critical for medical treatment and environmental governance. Here, we show that our methodology can detect samples containing unknown nerve agent mimics and, through calibration curves, also infer their concentrations.

In Figure 8, fluoride and thiol autoamplification cascades in samples (1−9) were incubated with standards of DFP and DSM, respectively, across a range of concentrations near the expected concentration of the unknown analyte to generate calibration curves. Blind unknown samples were juxtaposed in the same 96-well plates as the calibration standards for imaging consistency.

Chromaticities from the calibration wells (1−9) were used to construct calibration curves in the xy space: each curve is a piecewise linear interpolation between each successive calibration well's representative chromaticities. Analyte concentrations for each unknown sample (a−h) was inferred by interpolation of the standard analytes as described above. For example, chromaticity of well c in Figure 8A is between that of calibration wells 5 and 6, with a median Euclidean distance in the xy space to well 5 = 0.024; to well 6 = 0.023. Color compositions for c is thus 0.024/(0.024 + 0.023) = 58.34% that of well 5 and 0.023/(0.024 + 0.023) = 41.65% that of well 6, resulting in [concentration of c] = 1.6 (ppm) × 58% + 2.0 (ppm) × 42% = 1.8 (ppm). The actual dose of analyte in well c was indeed 1.8 ppm. On the basis of the same methodology, all other wells containing unknown analytes were calculated to output the theoretical doses of DFP or DSM added to compare with the actual doses input as summarized in Table 1.

As noted in Table 1 and Table S1 (see Supporting Information), the calculation of standard deviation for error was 13%. Some of the errors are large (i.e., −26, −33, −51), likely due to variations in the times used to stop and dilute the reactions, because the signals from self-propagating cascades are very sensitive to the time set for analysis. Irrespective, we have thus demonstrated that our self-propagating cascades for ratiometric fluorescence signal amplification interpreted via image analysis using the CIE 1931 color space have potential for practical applications.

■ CONCLUSION

Fluoride and thiol self-propagating cascades were successfully employed for fluorometric signal amplification and differentiation of G- and V-series nerve agent mimics: DFP and DSM, respectively. An image analysis pipeline was developed to perform ratiometric fluorescence sensing using common

A

Table 1. Predictions of Unknown Samples Based on Chromaticity

	detection of G-series nerve agent mimic: DFP (ppm)				detection of V-series nerve agent mimic: DSM (ppm)		
well	cal.[a]	act.[b]	err.[c] (%)	well	cal.	act.	err. (%)
a.	1.9	2.6	−26	a.	0.5	0.5	0
b.	0.6	0.6	0	b.	2.0	2.5	−19
c.	1.8	1.8	0	c.	1.6	1.8	−10
d.	3.0	3.6	−16	d.	3.6	4.3	−16
e.	1.6	1.4	+14	e.	0.5	1.0	−51
f.	3.1	4.0	−22	f.	2.6	3.3	−20
h.	2.4	3.4	−33	g.	1.7	2.0	−15
standard deviation for error = 13%				h.	2.1	2.8	−23
				i.	1.0	1.3	−23

[a]"cal." is abbreviation of "calculated". [b]"act." is abbreviation of "actual". [c]"err." is abbreviation of "error".

by interpolating calibration samples, were used to infer each reaction's analyte concentration. In essence, our device and method replace standard 96-well plate readers. Thus, our fluorescent self-propagating cascades and image processing result in a very simple and efficient portable use of common cell phones, with broad real-world field applications.

■ ASSOCIATED CONTENT

Ⓢ Supporting Information

The Supporting Information is available free of charge on the ACS Publications website at DOI: 10.1021/acscentsci.8b00193.

Experimental procedures and control experiments with figures (PDF)
LEGO dark-box construction instructions (PDF)

■ AUTHOR INFORMATION

Corresponding Authors
*(E.M.M.) E-mail: marcotte@icmb.utexas.edu.
*(E.V.A.) E-mail: anslyn@austin.utexas.edu.
ORCID Ⓘ
Xiaolong Sun: 0000-0003-4003-6924
Eric V. Anslyn: 0000-0002-5137-8797
Author Contributions
#X.S. and A.A.B. contributed equally.

Notes
The authors declare no competing financial interest.

B

■ ACKNOWLEDGMENTS

Figure 8. Fluorescence photo images; chromaticity for standard and unknown nerve agent mimics triggered self-propagating cascades. (A, inset) Wells 1−9 are standard samples of known DFP concentrations (0, 0.4, 0.8, 1.2, 1.6, 2.0, 2.4, 2.8, 3.2 ppm). Wells a−h are unknown samples. Fluoride self-propagating cascades were operated exactly as in Figure 6; (B, inset) Wells 1−9 are standard samples of known DSM concentrations (0, 0.76, 1.52, 2.28, 3.04, 3.80, 4.56, 5.32, 6.08 ppm). Wells a−i are unknown samples. Thiol self-propagating cascades were operated exactly as in Figure 7; (A, B, graph) Chromaticities of randomly sampled pixels from calibration wells 1−9 are represented as color-coded open circles. Chromaticities of randomly sampled pixels from the unknown samples are overlaid as points.

cellular phone images and an easily assembled field-deployable LEGO box. Pixel chromaticities for each cascade reaction were quantitatively mapped onto the CIE 1931 xyY color space and,

■ REFERENCES

(1) Sidell, F. R.; Borak, J. Chemical warfare agents: II. nerve agents. *Ann. Emerg. Med.* **1992**, *21*, 865−871.

(2) Wiener, S. W.; Hoffman, R. S. Nerve agents: a comprehensive review. *J. Intensive Care Med.* **2004**, *19*, 22−37.

(3) Royo, S.; Martinez-Manez, R.; Sancenon, F.; Costero, A. M.; Parra, M.; Gil, S. Chromogenic and fluorogenic reagents for chemical warfare nerve agents' detection. *Chem. Commun. (Cambridge, U. K.)* **2007**, 4839−4847.

(4) Swiderska, M. A.; Reymond, J.-L. Analytical chemistry: A dendritic signal amplifier. *Nat. Chem.* **2009**, *1*, 527−528.

(5) Sella, E.; Lubelski, A.; Klafter, J.; Shabat, D. Two-Component Dendritic Chain Reactions: Experiment and Theory. *J. Am. Chem. Soc.* **2010**, *132*, 3945−3952.

(6) Sella, E.; Weinstain, R.; Erez, R.; Burns, N. Z.; Baran, P. S.; Shabat, D. Sulfhydryl-based dendritic chain reaction. *Chem. Commun. (Cambridge, U. K.)* **2010**, *46*, 6575−6577.

(7) Baker, M. S.; Phillips, S. T. A Two-Component Small Molecule System for Activity-Based Detection and Signal Amplification: Application to the Visual Detection of Threshold Levels of Pd(II). *J. Am. Chem. Soc.* **2011**, *133*, 5170−5173.

(8) Yoshii, T.; Onogi, S.; Shigemitsu, H.; Hamachi, I. Chemically Reactive Supramolecular Hydrogel Coupled with a Signal Amplification System for Enhanced Analyte Sensitivity. *J. Am. Chem. Soc.* **2015**, *137*, 3360−3365.

(9) Sun, X. L.; Shabat, D.; Phillips, S. T.; Anslyn, E. V. Self-propagating amplification reactions for molecular detection and signal amplification: Advantages, pitfalls, and challenges. *J. Phys. Org. Chem.* **2018**, e3827.

(10) Sun, X.; Dahlhauser, S. D.; Anslyn, E. V. New Autoinductive Cascade for the Optical Sensing of Fluoride: Application in the Detection of Phosphoryl Fluoride Nerve Agents. *J. Am. Chem. Soc.* **2017**, *139*, 4635−4638.

(11) Sun, X.; Reuther, J. F.; Phillips, S. T.; Anslyn, E. V. Coupling Activity-Based Detection, Target Amplification, Colorimetric and Fluorometric Signal Amplification, for Quantitative Chemosensing of Fluoride Generated from Nerve Agents. *Chem. - Eur. J.* **2017**, *23*, 3903−3909.

(12) Sun, X.; Anslyn, E. V. An Auto-Inductive Cascade for the Optical Sensing of Thiols in Aqueous Media: Application in the Detection of a VX Nerve Agent Mimic. *Angew. Chem.* **2017**, *129*, 9650−9654.

(13) Lee, M. H.; Kim, J. S.; Sessler, J. L. Small molecule-based ratiometric fluorescence probes for cations, anions, and biomolecules. *Chem. Soc. Rev.* **2015**, *44*, 4185−4191.

(14) Maruyama, S.; Kikuchi, K.; Hirano, T.; Urano, Y.; Nagano, T. A Novel, Cell-Permeable, Fluorescent Probe for Ratiometric Imaging of Zinc Ion. *J. Am. Chem. Soc.* **2002**, *124*, 10650−10651.

(15) Kiyose, K.; Kojima, H.; Urano, Y.; Nagano, T. Development of a Ratiometric Fluorescent Zinc Ion Probe in Near-Infrared Region, Based on Tricarbocyanine Chromophore. *J. Am. Chem. Soc.* **2006**, *128*, 6548−6549.

(16) Komatsu, K.; Urano, Y.; Kojima, H.; Nagano, T. Development of an Iminocoumarin-Based Zinc Sensor Suitable for Ratiometric Fluorescence Imaging of Neuronal Zinc. *J. Am. Chem. Soc.* **2007**, *129*, 13447−13454.

(17) Wang, J.; Qian, X.; Cui, J. Detecting Hg2+ Ions with an ICT Fluorescent Sensor Molecule: Remarkable Emission Spectra Shift and Unique Selectivity. *J. Org. Chem.* **2006**, *71*, 4308−4311.

(18) Zhang, X.; Xiao, Y.; Qian, X. A Ratiometric Fluorescent Probe Based on FRET for Imaging Hg2+ Ions in Living Cells. *Angew. Chem., Int. Ed.* **2008**, *47*, 8025−8029.

(19) Xu, Z.; Xiao, Y.; Qian, X.; Cui, J.; Cui, D. Ratiometric and Selective Fluorescent Sensor for CuII Based on Internal Charge Transfer (ICT). *Org. Lett.* **2005**, *7*, 889−892.

(20) Qian, X.; Xiao, Y.; Xu, Y.; Guo, X.; Qian, J.; Zhu, W. "Alive" dyes as fluorescent sensors: fluorophore, mechanism, receptor and images in living cells. *Chem. Commun.* **2010**, *46*, 6418−6436.

(21) Krüger, J.; Singh, K.; O'Neill, A.; Jackson, C.; Morrison, A.; O'Brien, P. Development of a microfluidic device for fluorescence activated cell sorting. *J. Micromech. Microeng.* **2002**, *12*, 486.

(22) Zhu, H.; Mavandadi, S.; Coskun, A. F.; Yaglidere, O.; Ozcan, A. Optofluidic Fluorescent Imaging Cytometry on a Cell Phone. *Anal. Chem.* **2011**, *83*, 6641−6647.

(23) Martinez, A. W.; Phillips, S. T.; Whitesides, G. M.; Carrilho, E. Diagnostics for the Developing World: Microfluidic Paper-Based Analytical Devices. *Anal. Chem.* **2010**, *82*, 3−10.

(24) Martinez, A. W.; Phillips, S. T.; Carrilho, E.; Thomas, S. W.; Sindi, H.; Whitesides, G. M. Simple Telemedicine for Developing Regions: Camera Phones and Paper-Based Microfluidic Devices for Real-Time, Off-Site Diagnosis. *Anal. Chem.* **2008**, *80*, 3699−3707.

(25) Asheim, J.; Kvittingen, E. V.; Kvittingen, L.; Verley, R. A Simple, Small-Scale Lego Colorimeter with a Light-Emitting Diode (LED) Used as Detector. *J. Chem. Educ.* **2014**, *91*, 1037−1039.

(26) Hunt, R. W. G.; Pointer, M. R. *Measuring Colour*; John Wiley & Sons: New York City, 2011.

(27) Marcotegui, B.; Beucher, S. Fast Implementation of Waterfall Based on Graphs. In *Mathematical Morphology: 40 Years On*; Springer: Berlin, 2005; pp 177−186.

(28) Titiwai is the Māori name for *Arachnocampa luminosa*, a bioluminescent glowworm that dwells in caves and grottoes in New Zealand.

(29) Shrivastava, A.; Gupta, V. B. Methods for the determination of limit of detection and limit of quantitation of the analytical methods. *Chron. Young Sci.* **2011**, *2*, 21.